Effect of various oxide additives on sintering of BaO–SiO$_2$ system glass-ceramics

S. SRIDHARAN
Ceramaseal, Division of Ceramx Corporation, New Lebanon, NY 12125, USA

M. TOMOZAWA
Materials Engineering Department, Rensselaer Polytechnic Institute, Troy, NY 12180, USA

Glass-ceramics can be produced by sintering and crystallization of a pressed glass powder pellet. Crystallization prior to complete densification results in a porous glass-ceramic. A small quantity of various oxides was added to and melted with 35.7 BaO–64.3 SiO$_2$ (mol %) glass and the sintering characteristic of the glass powder was evaluated in terms of the density relative to the bulk glass density after heating at a constant rate. Some oxide additives, such as Al$_2$O$_3$ and ZrO$_2$, increased the per cent relative density while others, such as Na$_2$O, decreased it. The achieved per cent relative density was compared with crystallization characteristics determined by differential thermal analysis (DTA) and viscosity determined by the beam-bending method. The per cent relative density showed a good correlation with the viscosity at the crystallization temperature, the higher per cent relative density being achieved for systems with the lower viscosity at the crystallization temperature.

1. Introduction

Glass-ceramics can be produced either by bulk crystallization of formed glass objects [1, 2] or by sintering and crystallization of pressed glass powders [3–12] in one heat treatment. The latter method is useful for producing refractory glass-ceramics without melting refractory glasses.

Sintering a glass-ceramic composition can be done either before crystallization by viscous sintering of glass [5] or after crystallization by diffusion sintering of crystallized glass-ceramic powders [13]. The crystallization peak temperature, T_p, in the differential thermal analysis (DTA) (cf. Fig. 1) trace of the glass separates the two processes, the sintering temperature being less than T_p for viscous sintering and greater than T_p for diffusion sintering. Because of relatively lower sintering temperatures and higher densification rates of viscous sintering [14], sintering of glass before crystallization is preferred.

Viscous sintering of a glass can be done either isothermally [10] or at constant heating rate (CHR) [5, 11]. Sintering is usually impeded by crystallization [11]. Thus under CHR sintering, sintering can be expected to proceed up to T_p. The viscous sintering rate is inversely related to viscosity of the glass, and because CHR can shift T_p to higher values compared to isothermal sintering, lower viscosity regions can be accessed before crystallization. Thus CHR sintering is especially suitable for sintering glass-ceramics.

The crystallization peak temperature, T_p, is a function of composition and heating rate. At a given heating rate, additions of a small quantity of other oxides to a base glass composition can significantly alter the T_p, consequently altering the sintering rate of the base glass. Because the viscosity of a glass decreases exponentially with increasing temperature, small variations in T_p with composition will cause large variations in viscosity at the crystallization peak temperature. As CHR sintering can proceed up to the crystallization peak temperature, the viscosity at the crystallization peak temperature, η_{T_p}, might be a good measure of the sinterability of glass-ceramics. In addition to the crystallization peak temperature, T_p, the crystallization start temperature, T_x, and crystallization completion temperature, T_{xc}, (cf. Fig. 1), can also be used for characterizing the crystallization. This paper attempts to establish the correlation between sinterability and the viscosity at a crystallization temperature.

The BaO–SiO$_2$ glass-ceramic system was chosen for this study because of its refractory nature, where the melting is not practical because of the extremely high temperatures involved [15].

2. Theory

Viscous sintering of a pressed glass pellet is treated separately in three microstructurally distinct stages, termed initial, intermediate and final. The microstructural processes in these three stages are elimination of negative curvatures between particles, reduction of open pore volume, and their eventual conversion to closed pores and reduction of closed pore volume, respectively. General isothermal densification kinetics equations have been derived by Frenkel (two spherical particles geometry) for the initial stage [16], by Scherer (cylindrical particles in different cell geometries) for initial and intermediate stages [17], and by Mackenzie and Shuttleworth (MS for short, spherical
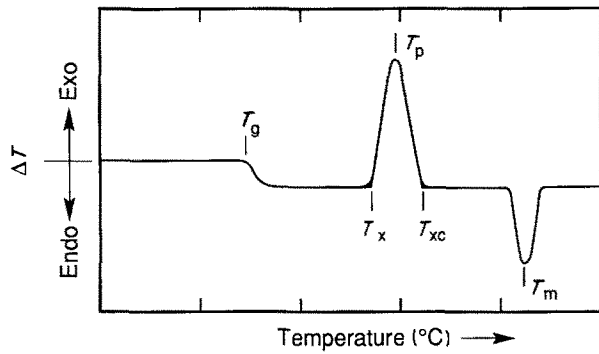
Figure 1 Schematic differential thermal analysis (DTA) trace for a glass-ceramic system. T_g = glass transition temperature; T_x = crystallization start temperature; T_p = crystallization peak temperature; T_{xc} = crystallization completion temperature; T_m = crystal melting temperature.

closed pores geometry) for final stage [18]. These can be expressed in differential form as

$$\frac{1}{3}\frac{d\ln\rho}{dt} = \frac{\gamma}{2\eta R_0} \quad \text{(Frenkel equation)} \tag{1a}$$

$$= \frac{\gamma n^{1/3}}{\eta}[(2C_1 - 3C_2 x)]/[(6x^{1/3}$$

$$\times (C_1 - C_2 x)^{2/3}]\,\text{(Scherer equation)} \tag{1b}$$

$$= [\gamma n_{MS}^{1/3}/2\eta]\left(\frac{4\pi}{3}\right)^{1/3}[(1/\rho) - 1]^{2/3}$$

$$\text{(MS equation)} \tag{1c}$$

where ρ is the relative (to density of the bulk glass) density of the sample, γ is the glass surface free energy, η is the viscosity of the glass at temperature T, R_0 is the initial particle size (radius), n the number of pores per unit volume of the solid phase and is related to the volume of the solid material in a unit cell having a single pore, V_s, by $n = 1/V_s$. C_1, C_2 are geometric constants of the model, $x = a/L$, where a and L are the radius and length of the cylinder, n_{MS} is the number of closed pores per unit volume of the solid material, and d/dt is the time derivative.

Among the various parameters in Equations 1a–c, ones which change with glass compositions would be surface energy, γ, and viscosity, η. Thus the overall densification of a glass compact with identical geometry but different composition should be given by

$$dF(\rho)/dt = (C\gamma/\eta) \tag{2}$$

where C is a constant and $F(\rho)$ is a function of relative density which increases with increasing relative density. Furthermore, variation of the surface energy, γ, with temperature [19] and glass composition [20] is negligibly small compared with that of viscosity. In CHR sintering, using the heating rate $K = dT/dt$

$$dF(\rho) = (C\gamma/K)(dT/\eta) \tag{3}$$

where $(C\gamma/K)$ can be regarded as a constant.

The viscosity of most of the silicate glasses follow Fulcher's equation [21], i.e.

$$\log \eta = A + B/(T - T_0) \tag{4}$$

where A, B and T_0 are material constants. Substituting this relation into Equation 3 and integrating in the

range of ρ_0–ρ_{T_f} and T_0–T_f, the densification can be given by

$$F(\rho_{T_f}) - F(\rho_0) = (C'\gamma/K)[(T_f - T_0)^2/B\eta_{T_f}] \tag{5}$$

where C' is a new constant, T_f is the final temperature and ρ_{T_f} and η_{T_f} are the relative density and viscosity at that temperature. (To obtain Equation 5, the relationship

$$\int_{T_0}^{T_f} dT/\eta \approx [(T_f - T_0)^2/(2.303\, B\, \eta_{T_f})]$$

has been used. This integral has been evaluated in Appendix A.)

Once the crystallization takes place the sintering process practically stops and the maximum sintering temperature becomes the crystallization peak temperature, T_p. Thus

$$F(\rho_{T_p}) - F(\rho_0) = [C'\gamma/K][(T_p - T_0)^2/B\eta_{T_p}] \tag{6}$$

Because the variation of $(T_p - T_0)^2/B$ with composition is much smaller than that of viscosity, this equation indicates that the most important factor in CHR sintering of crystallizable glasses is the viscosity at the crystallization temperature.

3. Experimental procedure

The base glass composition chosen for this study was 35.7 BaO–64.3 SiO$_2$ (mol %), with an SiO$_2$/BaO ratio of 1.8 and designated BG, which lies in the middle of the two-phase field BS$_2$–B$_3$S$_5$(B = BaO, S = SiO$_2$), in the BaO–SiO$_2$ binary [15]. Glasses with additives such as Al$_2$O$_3$, ZrO$_2$, B$_2$O$_3$, Na$_2$O, K$_2$O, BaO, TiO$_2$, SiO$_2$ and P$_2$O$_5$ were prepared. The compositions studied are shown in Table I.

Appropriate mole per cents of component powders, including additives, were mixed in ethanol and stirred for 1 h to achieve homogeneity in mixing. Then the ethanol was evaporated in an air oven held at $\approx 70\,°C$. Melting was done at 1550–1600 °C, in a CM rapid-temperature furnace, using a 60 ml Pt–20% Rh crucible, for about 6 h. The melts were poured into a brass mould and allowed to cool to room temperature. The bulk glasses thus produced were annealed at 700–720 °C for 1 h and furnace cooled to room temperature.

Bulk glasses were crushed and sieved in between 270 and 400 mesh screens to obtain the estimated particle size range 38–53 μm. Differential thermal analysis (DTA) was conducted on these powders, at 10 °C min^{-1} heating rate, using a Perkin–Elmer 1700 model. The amount of the powder used was 70–90 mg.

Pellets of size 0.572 cm (diameter) × 0.635 cm (height), were uniaxially cold pressed at 207 MPa pressure without binder. Binder was purposely avoided to eliminate differential densification caused by the removal of binder [22]. Pressed pellets were immersed in distilled water during which any delaminated layers (occurring during compaction) fell out of the compact. Subsequently, the compacts were dried in air at ~70 °C for ~10 h. Sintering was done in a CM rapid furnace fitted with a programmable

TABLE I Composition, DTA crystallization and CHR sintering data for glasses studied

Glass		Composition		DTA results[a]		CHR sintering results[a]		
No.	Code	SiO_2/BaO ratio	Others (mol %)	T_x ($\pm$ 5 °C)	T_p	D_g	ρ_{T_x} (%)	ρ_{T_p} (%)
1	BG	1.8	–	839	866	3.80	87.2	89.2
Set A								
2	BGP 2.5	1.8	$2.5(P_2O_5)$	895	937	3.73		90.9
3	BGZ 2.5	1.8	$2.5(ZrO_2)$	893	931	3.90	94.4	92.3
4	BGB 2.5	1.8	$2.5(B_2O_3)$	833	849	3.82	89.9	88.7
5	BGA 2.5	1.8	$2.5(Al_2O_3)$	877	913	3.76	96.8	94.9
6	BGK 2.5	1.8	$2.5(K_2O)$	816	858	3.76	86.3	89.1
7	BGN 2.5	1.8	$2.5(Na_2O)$	753	765	3.91	80.6	81.1
8	BGS 2.5	1.8	$2.5(SiO_2)$	835	860	3.77	90.5	93.1
9	BGBa 2.5	1.8	$2.5(BaO)$	832	844	3.86		91.2
10	BGT 2.5	1.8	$2.5(TiO_2)$	850	868	3.87		89.8
Set B								
11	BGA 1.25	1.8	$1.25(Al_2O_3)$	830	898	3.78		95.0
12	BGA 5	1.8	$5.0(Al_2O_3)$	911	980	3.72	97.2	96.5
13	BGA 7.5	1.8	$7.5(Al_2O_3)$	980	980[b]	3.67	98.1	98.1
14	BGA 10	1.8	$10(Al_2O_3)$	1000	1000[b]	3.63	99.0	99.0
15	BGZ 5	1.8	$5.0 (ZrO_2)$	943	990	3.92	95.7	93.4
16	BGZ 7.5	1.8	$7.5(ZrO_2)$	984	1033	3.95	94.7	96.2
17	BGZ 10	1.8	$10(ZrO_2)$	1065	1090	3.98	97.6	98.0
18	BGS 5	1.8	$5.0(SiO_2)$	826	847	3.74	89.4	90.4
19	BGB 5	1.8	$5.0(B_2O_3)$	807	829	3.85	83.4	85.5
20	BGP 5	1.8	$5.0(P_2O_5)$	922	944[c]			
21	BGP 0.75	1.8	$0.75(P_2O_5)$	858	874	3.82		96.1
22	BGP 1.5	1.8	$1.50(P_2O_5)$	884	898	3.79		96.0
23	BGP 2.25	1.8	$2.25(P_2O_5)$	894	911	3.74	95.9	95.7
24	BGS 6.67	1.8	$6.67(SiO_2)$	835	845	3.74		87.2

[a] Heating rate 10 °C min^{-1}; estimated particle size range 38–53 μm.
[b] DTA scan did not have discernable crystallization peak, only a hump due to densification observed. The temperature corresponding to the end of the hump was taken.
[c] Visibly phase separated on cooling to room temperature.

controller. Pellets were placed on an alumina plate and heated at 10 °C min^{-1} up to the desired temperature, T_x or $T_p \pm 1$ °C, and then furnace cooled.

The density of a glass, D_g, was measured using a 1 cm × 1 cm × 1 cm cube of the annealed glass by Archimedes' method, in distilled water. For the density of the pressed as well as sintered pellet, the pellet was first weighed in air, M g. Then it was immersed in distilled water and the entrapped air in the pores was sucked out by a mechanical pump and maintained under vacuum for 1 h. Then the chamber was suddenly vented to the atmosphere to force water into the small pores, and the pellet was allowed to remain under water for an additional hour. The water-soaked weight was measured in air, S g. The immersed weight of the pellet was also measured using water as the medium, I g. The bulk density was calculated according to the formula [23]

$$D_{bulk} = M/(S - I) \qquad (7)$$

and the relative density was calculated in terms of the glass density as

$$\%\rho = (D_{bulk}/D_g) \times 100 \qquad (8)$$

For each data point a minimum of three pellets was sintered and the average of their densities was taken. The variation in initial relative density, (ρ_0) was $\pm$ 3% and that in sintered relative density $(\rho_{T_p \text{ or } T_x})$ was $\pm$ 2%.

The viscosity of glasses in the range 10^9–10^{13} P was measured by the beam-bending method [24, 25]. Samples of size 0.445 cm (height) × 0.610 cm (width) × ~ 4.166 cm (length) were cut from the annealed bulk glass. The sample surface that was in contact with the platinum supports was polished down to the 1 μm level to eliminate friction between the sample and support which could increase the observed viscosity values. The span used was 3.125 cm. The sample temperature was maintained, along its length, within $\pm$ 2 °C. The running conditions were tested with NBS 711 and NBS 717 standard glasses [26, 27]. The observed difference between log $\eta_{measured}$ and log $\eta_{NBS \ standard}$ (P) was 0.20 in 3σ, where σ is the standard deviation of the difference in log η.

For selected samples, dilatometric shrinkage curves were obtained at the heating rate of 10 °C min^{-1} using pressed samples of ball-milled powders. The fine ball-milled powder had to be used in order to prepare samples strong enough not to crumble during the dilatometric measurement. The corresponding crystallization temperatures of the same ball-milled powders were also obtained by performing DTA scans at 10 °C min^{-1}.

4. Results and discussion

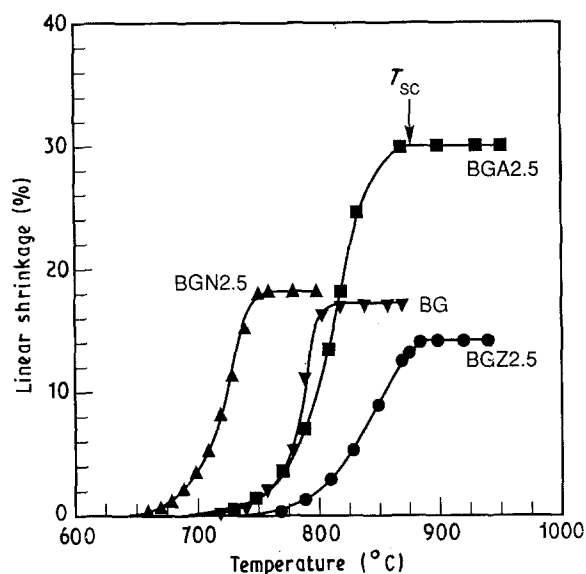Dilatometric shrinkage curves obtained for selected samples are shown in Fig. 2. The sintering completion

Figure 2 Selected dilatometric shrinkage curves of ball-milled glass powders, at CHR of 10 °C min⁻¹. T_{sc} = sintering completion temperature; for glass codes refer to Table I.
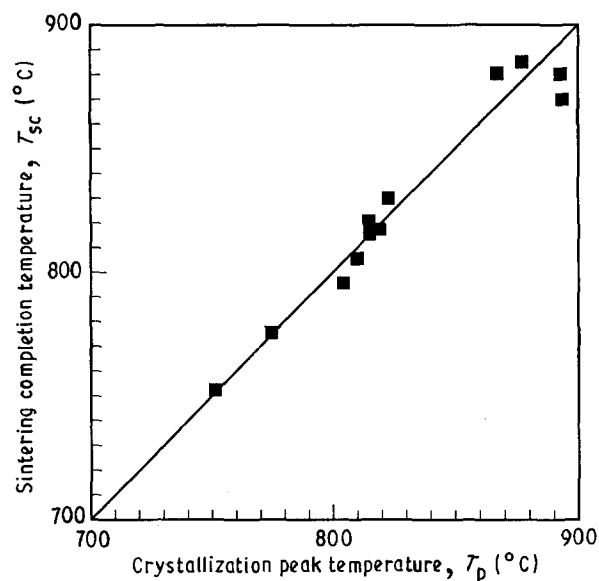

Figure 3 Comparison of dilatometry sintering completion temperature, T_{sc}, to the DTA crystallization peak temperature, T_p. Both temperatures were obtained at CHR of 10 °C min⁻¹ using ball-milled powders.

TABLE II Dilatometric data versus DTA results[a]

Glass	Apparent maximum linear shrinkage (%)	T_{sc}^b (°C)	T_p^c (°C)	$\text{Log } \eta_{T_p}$
BG	17.0	805	800	8.70
BGZ 2.5	14.1	885	857	8.25
BGB 2.5	22.0	815	807	8.38
BGA 2.5	29.9	870	867	7.52
BGK 2.5	21.4	775	768	9.03
BGN 2.5	18.1	752	747	9.13
BGS 2.5	18.7	817	812	8.33
BGT 2.5	16.1	830	816	
BGA 5	16.6	860	885	7.80
BGB 5	16.5	795	793	8.85
BGS 5	18.7	820	809	8.51
BGP 2.25	22.9	880	856	7.35

[a] On ball-milled powder at 10 °C min⁻¹.
[b] Sintering completion temperature from dilatometry.
[c] DTA crystallization peak temperature.

temperature, T_{sc}, is indicated in the figure and is tabulated in Table II, together with the crystallization peak temperature, T_p, obtained from DTA using the same glass powder heated at the same heating rate (10 °C min⁻¹). All the glasses in Table II sintered to less than full density. These two temperatures are compared in Fig. 3. From the figure it can be seen that the sintering completion temperature coincides with the DTA peak temperature, within experimental errors of T_p, ± 5 °C.

4.1. Characterization of viscosities at crystallization temperatures

The beam-bending viscosity data for selected glasses are shown in Fig. 4. In order to determine the viscosity at crystallization temperature, which is outside the measured range, the temperature dependence of the viscosity, η, was fitted by Fulcher's equation (cf. Equation 4).
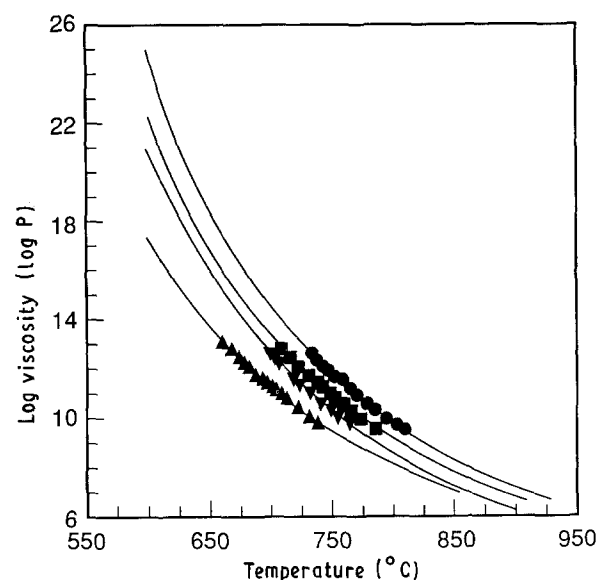

Figure 4 Viscosity–temperature data for few glasses. Marks are observed beam-bending data, solid lines are Fulcher's equation fit extrapolated up to T_p. For glass codes refer to Table I. (▼) BG, (●) BGZ 2.5, (■) BGA 2.5, (▲) BGK 2.5.

Because a narrow region of the η–T plot is measured, to fit reliably to Fulcher's equation, a data point far away from the region of measurements or a Fulcher's constant, T_0, is needed. In order to estimate T_0 from T_g, which can be measured, T_g/T_0 versus mol % glass formers (%GF) of various oxide glasses reported in the literature [21, 26–33] was plotted in Fig. 5. The justification for Fig. 5 is made in Appendix B. In the region of interest, i.e. 57.9–66.7 mol % glass formers, the T_g/T_0 ratio, expressed in K K⁻¹, depends on mole per cent glass former as

$$T_g/T_0 = 0.0125(\%GF) + 0.62 \qquad (9)$$

For three BaO–SiO₂ glasses, the experimentally observed low temperature viscosity data of current
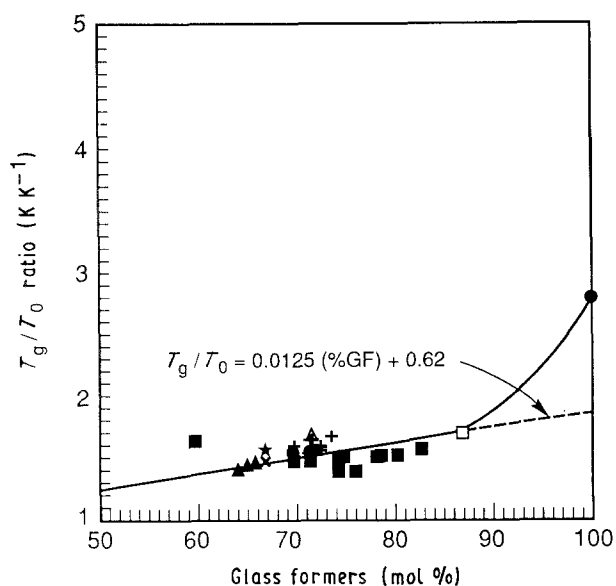
Figure 5 T_g/T_0 versus mol % GF plot for silicate glasses. (●) SiO_2 glass, (△) NBS 711 glass, (+) container glasses, (×) $K_2O \cdot 2SiO_2$ glass, (▲) barium silicate glasses, (□) NBS 717 glass, (■) Fulcher's glasses, (●) Lillie's glasses, (★) $Na_2O \cdot 2SiO_2$ glass.

research and the melt viscosity data from the literature [34] were fitted to Fulcher's equation, using the least square refining method [35]. The resulting T_g/T_0 values, of 1.41, 1.44 and 1.46 with the respective mole per cent glass former being 64.3, 65.2 and 66.1, agree very well with Fig. 5.

For the present series of glasses, T_g at log $\eta = 13$ was deduced from the observed beam-bending data $(10^9–10^{13})$. With the known values of T_g and mol % GF, using Equation 9, T_0 was obtained. With this T_0 value the observed η–T data were fitted to Fulcher's equation, using the least square refining method. The results are shown in Fig. 4 and are tabulated in Table III along with the calculated viscosities at two different crystallization characteristic temperatures, namely, the crystallization start temper-

ature, T_x, and the crystallization peak temperature, T_p. The average 3σ (σ is the standard deviation) in log η of the fit is 0.16. This range in 3σ is well within that (0.20) observed for the NBS standard glasses.

4.2. Characterization of CHR sintering

Crystallization characteristics determined from DTA and CHR sintering results are shown in Table I for various glasses. The initial relative density, ρ_0, with $68.7 \pm 3\%$, was nearly constant, independent of composition. First the sintering characteristics were evaluated for the glasses with 2.5 mol % oxide additions to the base glass (BG) (cf. Table I, set A). Noting the beneficial effects of certain oxides, the investigation was extended to higher mole per cents for certain oxide additives to BG (cf. Table I, set B). The results are plotted in Fig. 6, in terms of the relative density achieved. From Fig. 6, it can be seen that additions of alumina and zirconia to the base glass increase greatly the per cent relative density achieved on sintering to T_p (% ρ_{T_p}). Small amounts of P_2O_5 increase it, while larger amounts decrease it. In fact the composition BGP5.0, having 5 mol % P_2O_5, producing white glass pieces on cooling (possibly phase separated), did not sinter at all. It appears that the observed maximum in Fig. 6 for P_2O_5 additions is due to a phase-separation effect on sintering. Addition of Na_2O decreases the per cent ρ_{T_p} achieved and those of K_2O, BaO, B_2O_3, TiO_2 and SiO_2 have minimum effect.

4.3. CHR sintering versus crystallization viscosities

Fig. 7 is a plot of per cent ρ_{T_p} against viscosity (η_{T_p}) at the crystallization peak temperature. It shows that lower the η_{T_p}, the higher is the per cent ρ_{T_p} achieved, supporting Equation 6, although the data scatters for percent $\rho_{T_p} > 95$.

TABLE III Viscosity data for selected glasses

Glass		Fulcher's equation constants			Crystallization viscosities[a]	
No.	Code	A	B	$T_0(°C)$	Log η_{T_x}	Log η_{T_p}
1	BG	− 3.074	4621.6	407.5	7.64	7.01
2	BGP 2.5	− 2.849	4733.0	398.9	6.69	5.95
3	BGZ 2.5	− 2.216	4372.4	439.3	7.42	6.68
4	BGB 2.5	− 3.332	4814.9	395.8	7.68	7.29
5	BGA 2.5	− 2.159	4265.8	426.1	7.30	6.60
6	BGK 2.5	− 1.225	3821.9	395.3	7.86	7.03
7	BGN 2.5	− 0.146	3837.4	333.5	9.00	8.75
8	BGS 2.5	− 3.310	4820.4	398.0	7.72	7.12
12	BGA 5	− 1.585	4069.2	451.5	7.27	6.11
13	BGA 7.5	− 0.470	3697.9	484.0	6.99	6.99
14	BGA 10	− 0.006	3469.2	496.8	6.84	6.84
15	BGZ 5	− 1.819	4216.6	472.1	7.14	6.32
16	BGZ 7.5	− 2.200	4392.1	521.6	7.30	6.39
17	BGZ 10	− 1.224	4050.1	550.6	6.65	6.28
18	BGS 5	− 2.705	4704.5	389.7	8.08	7.58
19	BGB 5	− 3.860	5079.6	393.3	8.42	7.80
23	BGP 2.25	− 3.003	4693.9	402.6	6.55	6.23

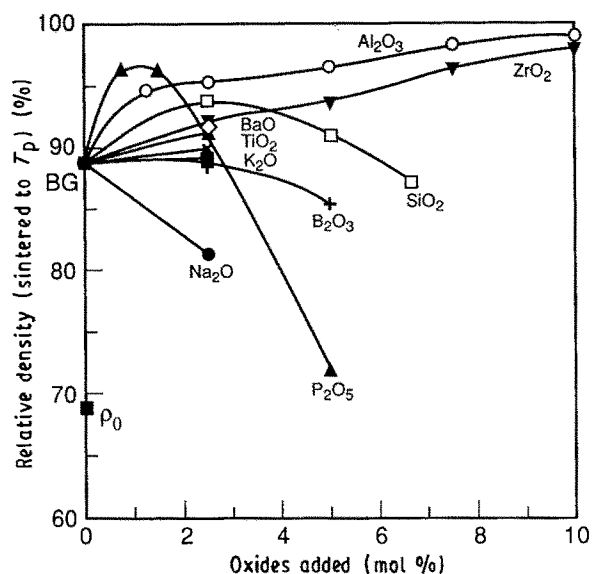[a] For estimated particle size range 38–53 μm at 10 °C min^{-1}.

Figure 6 Effect of oxide additions to the base glass, BG, on the sintered density. (ρ_0 = average initial % relative density; 270–400 mesh powder was heated up to T_p at CHR of $10\,°C\,min^{-1}$.

Figure 7 Sintered density (% ρ_{T_p}) versus viscosity at the crystallization peak temperature η_{T_p}, for CHR ($10\,°C\,min^{-1}$) sintering to T_p (270–400 mesh powder).

The scatter in per cent $\rho_{T_p} > 95$ data, especially Glasses 13 and 14 in Fig. 7, might be due to differing volume fractions of crystals for various glasses sintered to T_p. The error associated with normalizing the sintered density with respect to the density of glasses without taking into account the density of crystalline species present, might give rise to scatter in the data. Also, in the temperature region $T_x - T_p$ (cf. Fig. 1), viscosity of the sample can increase due to crystallization, whereas viscosity at T_p was estimated without considering the effect of crystallization. These difficulties should be minimized when per cent relative density obtained by sintering to the crystallization start temperature, T_x, (% ρ_{T_x}), is compared to the viscosity at that temperature, (η_{T_x}). The glasses in Fig. 7 were sintered up to T_x and the results are plotted in Fig. 8. The scatter in the per cent $\rho_{T_x} > 95$ is indeed lower in Fig. 8, compared with that in Fig. 7.

Comparison of per cent ρ_{T_x} with per cent ρ_{T_p} data in Table I reveals that only a small amount of sintering occurs beyond T_x, indicating that viscosity at the crystallization start temperature, (η_{T_x}), is a better parameter than the viscosity at the crystallization peak temperature, (η_{T_p}). Consistently the dilatometric data shown in Fig. 2 show the slowing down of the shrinkage rate when the temperature approaches the sintering completion temperature, which is nearly the same as T_p.

It might be speculated that the apparent maximum per cent linear shrinkage shown in Fig. 2 would correlate with the viscosity at the sintering completion temperature, T_{sc}, or the crystallization peak temperature, T_p, shown in Table II. Although the apparent maximum per cent linear shrinkage increases as the viscosity at the crystallization peak temperature decreases, the data scatter a lot. This might be due to the maximum linear shrinkage observed in dilatometry being a combination of two effects, (i) shrinkage due to densification of the sample, and (ii) shrinkage due to viscous flow of the glass under the dilatometer spring
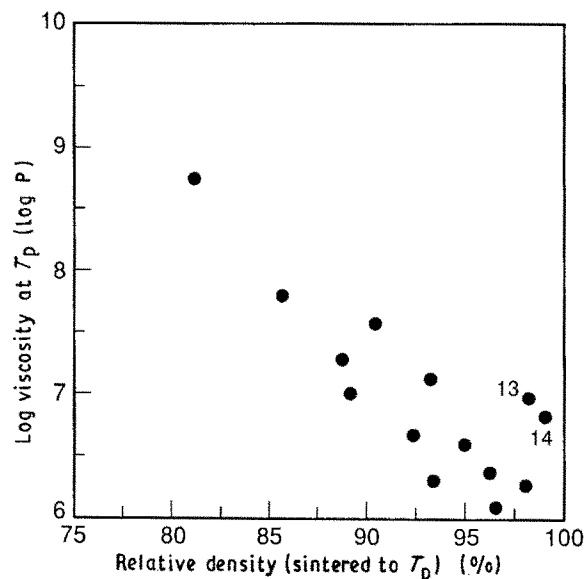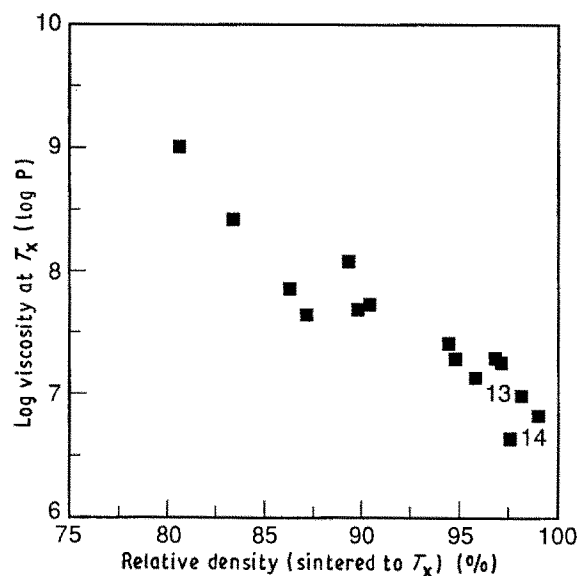

Figure 8 Sintered density (% ρ_{T_x}) versus viscosity at the crystallization start temperature, η_{T_x}, for CHR ($10\,°C\,min^{-1}$) sintering to T_x (270–400 mesh powder).

load. The densification part of the apparent linear shrinkage can be deduced only when both axial and radial strains are measured simultaneously [36–38].

5. Conclusions

1. The CHR sintering of glasses practically stops at the crystallization temperature.

2. Additions of Al_2O_3 and ZrO_2 to 35.7 BaO–64.3 SiO_2 (mol %) glass increase the sinterability, that of Na_2O decreases it and those of TiO_2, BaO, B_2O_3, K_2O and SiO_2 have marginal effects. Further, small additions (up to ~ 0.8 mol %) of P_2O_5 increase the sinterability while larger additions decrease it considerably due to probable phase separation.

3. The per cent relative sintered density achieved has an inverse relationship with the viscosity at the crystallization temperature, namely, the lower the vis-

cosity at the crystallization temperature, the higher is the sintered density achieved.

4. Of the two temperatures characteristic of crystallization, namely, crystallization start temperature (T_x) and crystallization peak temperature (T_p), T_x is more relevant in determining sinterability, i.e. the viscosity at the crystallization start temperature, (η_{T_x}), has better correlation with the viscous sinterability of crystallizable glass systems.

Acknowledgements

Appendix A. Derivation of $\int_{T_0}^{T_f} dT/\eta \approx [(T_f - T_0)^2/(2.303\ B\eta_{T_f})]$

Fulcher's equation is

$$\log \eta = A + [B/(T - T_0)] \tag{A1}$$

Substituting $A' = e^{2.303A}$ and $B' = 2.303B$, Equation A1 can be expressed as

$$\eta = A'e^{B'/(T - T_0)} \tag{A2}$$

Thus

$$\int dT/\eta = \int dT/\{A'e^{B'/(T - T_0)}\} \tag{A3}$$

Letting

$$\ln y = -B'/(T - T_0) \text{ or } y = e^{-B'/(T - T_0)} \tag{A4}$$

and differentiating we get

$$d\ln y = (\ln^2 y/B')dT \tag{A5}$$

Substitution of Equations A4 and A5 into Equation A3 gives

$$\int dT/\eta = [B'/A']\int dy/(\ln^2 y) \tag{A6}$$

The RHS integral in Equation A6 can be evaluated and approximated as follows

$$\int dy/[\ln^2 y] = [y/(\ln^2 y)][1 + (2/\ln y) + (6/\ln^2 y)$$
$$+ (24/\ln^3 y) + \ldots] \approx y/(\ln^2 y) \tag{A7}$$

This approximation is valid in the present case, because the second and higher order terms are smaller than unity in the temperature range of interest, i.e. $T_0 - T_f$. The maximum magnitudes of the second and higher order terms correspond to $T_f \approx T_p$, and using the typical values of $B \approx 4000\,°C$, $T_0 \approx 500\,°C$ (cf. Table III) and $(T_p)_{max} \approx 1100\,°C$ (cf. Table I), $\ln y \approx -15$ (cf. Equation A4).

Substituting Equation A7 into Equation A6 and integrating in the range of $t_0 - T_f$ and $\eta_{T_0}[= \text{infinity}]$ to η_{T_f}, and substituting back $B = B'/2.303$, we get the equation in the text, namely

$$\int_{T_0}^{T_f} dT/\eta \approx [(T_f - T_0)^2/(2.303\ B\ \eta_{T_f})]$$

Appendix B. Justification of Fig. 5

There are theoretical attempts to predict the Fulcher's constant, T_0 [39, 40] based on excess entropy at glass transition temperature, $S_{ex,\ T_g}$, being finite and constant (cf. footnote p. 24 of [41]). $S_{ex,\ T_g}$ is defined as

$$S_{ex,\ T_g} = \int_{T_0}^{T_g} \Delta C_p\, d\ln T \tag{A8}$$

where $\Delta C_p = C_{p,l} - C_{p,g}$, $C_{p,l}$ is the heat capacity under constant pressure of liquid state and $C_{p,g}$ is the heat capacity under constant pressure of the glassy state. Reasonable approximation for ΔC_p proposed [40] is constant/T, where T is any temperature. Thus

$$\Delta C_p(T)T = \Delta C_p(T_g)T_g \tag{A9}$$

where $\Delta C_p(T_g)$ is the difference in the heat capacities of liquid state and glassy state at T_g. Substituting Equation A9 into Equation A8 one can derive

$$S_{ex,\ T_g} = \int_{T_0}^{T_g} \Delta C_p\, d\ln T$$
$$= \int_{T_0}^{T_g} [\Delta C_p(T_g) T_g/T]\, d\ln T$$
$$= \Delta C_p(T_g) T_g(-1/T)_{T_0}^{T_g}$$
$$= \Delta C_p(T_g) T_g[(1/T_0) - (1/T_g)]$$
$$= \Delta C_p(T_g)[(T_g/T_0) - 1] \tag{A10}$$

Equation A10 suggests that for the excess entropy at the glass transition temperature to be constant, as $\Delta C_p(T_g)\uparrow$, $[(T_g/T_0) - 1]\downarrow$. Because T_g/T_0 is always greater than one, $[T_g/T_0]$ has to decrease when $\Delta C_p(T_g)$ increases.

Strong network liquids, such as SiO_2, show little or no change in C_p at T_g (cf. Fig. 6, p. 39 of [41]). Thus for pure SiO_2 glass $\Delta C_p(T_g)$ is small and from Equation A10, for $S_{ex,\ T_g}$ to be constant, T_g/T_0 has to be large, in accordance with its nearly Arrhenius $\eta - T$ relationship. On the other hand, non-network liquids, such as lithium acetate (cf. Fig. 6, p. 39 of [41]), show large $\Delta C_p(T_g)$ and from Equation A10, for $S_{ex,\ T_g}$ to be constant, T_g/T_0 has to be small, in accordance with their observed non-Arrhenius $\eta - T$ relationship. Because addition of network modifiers to SiO_2 glass degrades its network structure, one can approximate that as the mole per cent glass formers decreases in a silicate glass, its $\Delta C_p(T_g)$ will increase and consequently its T_g/T_0 ratio will decrease, to keep $S_{ex,\ T_g}$ constant. This is the trend observed in Fig. 5.

References

1. P. W. McMILLAN, in "Glass-Ceramics" (Academic Press, New York, 1979), pp. 97–142.
2. Z. STRNAD, in "Glass-ceramic materials", Glass Science and Technology, Vol. 8 (Elsevier, New York, 1986), pp. 114–126.
3. M. TASHIRO, *J. Non-Cryst. Solids* **73** (1985) 575.
4. E. M. RABINOVICH, *Amer. Ceram. Soc. Bull.* **58** (1979) 595.
5. S. KNICKERBOCKER, M. R. TUZZOLO and S. LAWHORNE, *J. Amer. Ceram. Soc.* **72** (1989) 1873.
6. E. M. RABINOVICH, *Inorg. Mater.* **7** (1971) 479.
7. A. H. KUMAR and R. R. TUMMALA, *Amer. Ceram. Soc. Bull.* **57** (1978) 738.
8. B. H. MUSSLER and M. W. SHAFER, *ibid.* **63** (1984) 705.

9. K. WATANABE and E. A. GIESS, *J. Amer. Ceram. Soc.* **68** (1985) C-102.
10. M. A. McCOY and A. H. HEUER, *ibid.* **71** (1988) 673.
11. P. C. PANDA and R. RAJ, *ibid.* **72** (1989) 1564.
12. B. H. MUSSLER and M. W. SHAFER, *Amer. Ceram. Soc. Bull.* **64** (1985) 1459.
13. W. SEMAR, W. PANNHORST, T. M. HARE and H. PALMOUR III, *Glastech. Ber.* **62** (1989) 74.
14. G. C. KUCZYNSKI, *J. Appl. Phys.* **20** (1949) 1160.
15. E. M. LEVIN, C. R. ROBBINS and H. F. McMURDIE, in "Phase diagrams for Ceramists" (American Ceramic Society, Columbus, OH, 1964) Fig. 211.
16. J. FRENKEL, *J. Phys. (Moscow)* **9** (1945) 385.
17. G. W. SCHERER, *J. Amer. Ceram. Soc.* **74** (1991) 1523.
18. J. K. MACKENZIE and R. SHUTTLEWORTH, *Proc. Phys. Soc. (London)* **62** (12-B) (1949) 833.
19. E. A. GIESS, J. P. FLETCHER and L. W. HERRON, *J. Amer. Ceram. Soc.* **67** (1984) 549.
20. W. D. KINGERY, H. K. BOWEN and D. R. UHLMANN, in "Introduction to Ceramics", 2nd Edn (New York, 1976) Fig. 5.22, p. 207.
21. G. S. FULCHER, *J. Amer. Ceram. Soc.* **8** (1925) 339.
22. F. F. LANGE, B. I. DAVIS and E. WRIGHT, *ibid.* **69** (1986) 66.
23. R. GRIFFITHS and C. RADFORD, in "Calculations in Ceramics" (Maclaren, London, UK, 1965) p. 37.
24. H. E. HAGY, *J. Amer. Ceram. Soc.* **46** (1963) 93.
25. A. NAPOLITANO, J. H. SIMMONS, D. H. BLACKBURN and R. E. CHIDESTER, *J. Res. Nat. Bur. Staud.* **78A** (1974) 323.
26. A. NAPOLITANO and E. G. HAWKINS, in "Standard Reference Materials: Viscosity of a Standard Lead-Silica Glass" NBS Special Publication 260-11 (NBS, 1966) Washington, DC, USA.
27. *Idem*, in "Standard Reference Materials: Viscosity of a Standard Borosilicate Glass", NBS special publication 260-23 (NBS, 1970) Washington, DC, USA.
28. E. H. FONTANA and W. A. PLUMMER, *Phys. Chem. Glasses.* **7** (1966) 139.
29. H. A. ROBINSON and C. A. PETERSON, *J. Amer. Ceram. Soc.* **27** (1944) 129.
30. H. R. LILLIE, *ibid.* **14** (1931) 502.
31. G. S. MEILING and D. R. UHLMANN, *Phys. Chem. Glasses* **8** (1967) 62.
32. J. P. POOLE, *J. Amer. Ceram. Soc.* **32** (1949) 230.
33. G. S. FULCHER, *ibid.* **8** (1925) 789.
34. J. O'M. BOCKRIS, J. D. MACKENZIE and J. A. KITCHENER, *Faraday Soc.* **51** (1955) 1734.
35. P. B. MACEDO, in "Proceedings of a Symposium On Mechanical and Thermal Properties of Ceramics", NBS Special Publication 303 (NBS, 1968), Washington, DC, USA, p. 169.
36. K. R. VENKATACHARI and R. RAJ, *J. Amer. Ceram. Soc.* **69** (1986) 499.
37. R. RAJ, *ibid.* **65** (1982) C-46.
38. V. C. DUCAMP and R. RAJ, *ibid.* **72** (1989) 798.
39. C. A. ANGELL and K. J. RAO, *J. Chem. Phys.* **57** (1972) 470.
40. C. A. ANGELL and W. SICHINA, in "The glass transition and the nature of the glassy state", edited by M. Goldstein and R. Simha, Annals of the New York Academy of Sciences, Vol. 279 (1976) p. 53.
41. J. WONG and C. A. ANGELL, in "Glass Structure by Spectroscopy" (Marcel Dekker, New York, 1976).